Supporting Information for:

Rational Design of DNA Nanocarriers via Sequence and Length Modulation of Linker and Lock Domains: Insights from Coarse-Grained Simulations

Shima Danaeimoghaddam, and Reza Soheilifard*

Department of Mechanical Engineering, Hakim Sabzevari University, Sabzevar, Iran

*Corresponding Author: Email: r.soheilifard@hsu.ac.ir

This supplementary file provides supporting design, modeling, and validation data for the DNA origami nanocarrier and its hybrid DNA–protein simulations described in the main manuscript. The figures document the structural design workflow, closure protocol, protein coarse-graining validation, lock sequence variants, and sensitivity analyses relevant to the robustness of the simulation framework.

S1. DNA origami design and structural components

Figure S1 presents the complete Cadnano design of the DNA origami nanosheet, including scaffold routing, staple layout, and functional elements. Linker strands designed for thrombin attachment are highlighted in red and orange, while locking strands incorporate the AS1411 aptamer (green) and its complementary sequence (blue).

S2. Two-step nanosheet closure protocol

Figure S2 illustrates the two-step closure procedure of the nanosheet visualized in oxView. In the first step, a harmonic pulling bias was applied perpendicular to the nanosheet plane to bring opposing scaffold edges into contact. In the second step, complementary aptamer base pairing was mimicked by introducing harmonic traps between paired locking strands, resulting in the final locked configuration.

S3. Validation of coarse-grained thrombin model

Figure S3 shows the residue-level B-factor profile of the ANM thrombin model compared with experimental data from the PDB structure. The plot, obtained directly from the ANM–oxDNA package, validates the coarse-grained protein representation used in the hybrid simulations.

S4. Lock sequence variants

Figure S4 lists the sequences of the complementary lock–aptamer domains designed for duplex lengths of 3, 4, 5, and 6 base pairs. These variants were used to examine the relationship between lock length, stability, and unlocking kinetics in the temperature-dependent simulations.

S5. Sensitivity of linker stability to harmonic trap stiffness

To evaluate whether the harmonic restraints used to model DNA–protein coupling influence linker stability, a simplified sensitivity analysis was performed. In this control setup, a single thrombin molecule was tethered to a complementary single-stranded DNA linker via a harmonic trap, while the opposing DNA strand—representing the attachment site on the nanocarrier—was held fixed in space. This configuration

isolates the effect of trap stiffness on local base-pairing behavior without contributions from global nanocarrier deformation.

Equilibrium oxDNA simulations were carried out over a range of harmonic trap stiffness values (0.7, 7, 14, 70, and 140; oxDNA units), spanning more than two orders of magnitude. For each stiffness value, the number of correctly formed hydrogen bonds between the linker and its complementary strand was monitored during equilibration, and probability distributions were constructed.

Figure S5 shows that the lowest stiffness value (0.7) leads to a visibly broader and shifted hydrogen-bond distribution, indicating insufficient mechanical constraint and enhanced linker fluctuations. In contrast, for stiffness values of 7 and higher, the hydrogen-bond distributions converge, with nearly identical peak positions and widths. This convergence demonstrates that, above a modest stiffness threshold, the precise choice of trap stiffness does not significantly affect linker base-pairing stability.

Accordingly, the linker release dynamics reported in the main text are robust with respect to the harmonic restraint strength used for DNA–protein coupling and primarily reflect intrinsic effects of linker sequence, length, and nanocarrier conformation.

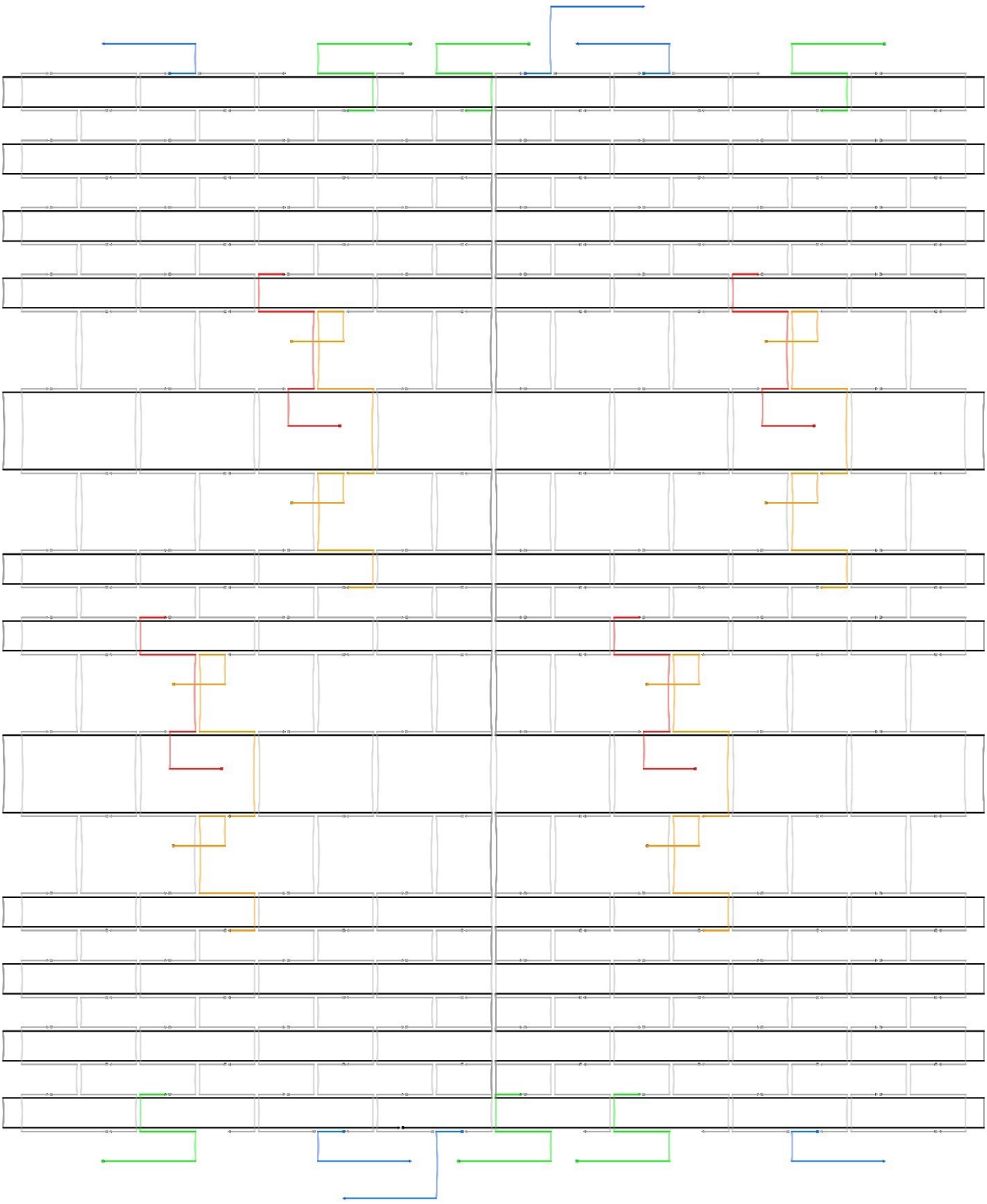

Figure S1. Cadnano design of the DNA origami nanosheet.

Complete design schematic showing scaffold and staple routing, linker strands for thrombin capture (red and orange), and locking strands incorporating the AS1411 aptamer (green) and its complementary sequence (blue).

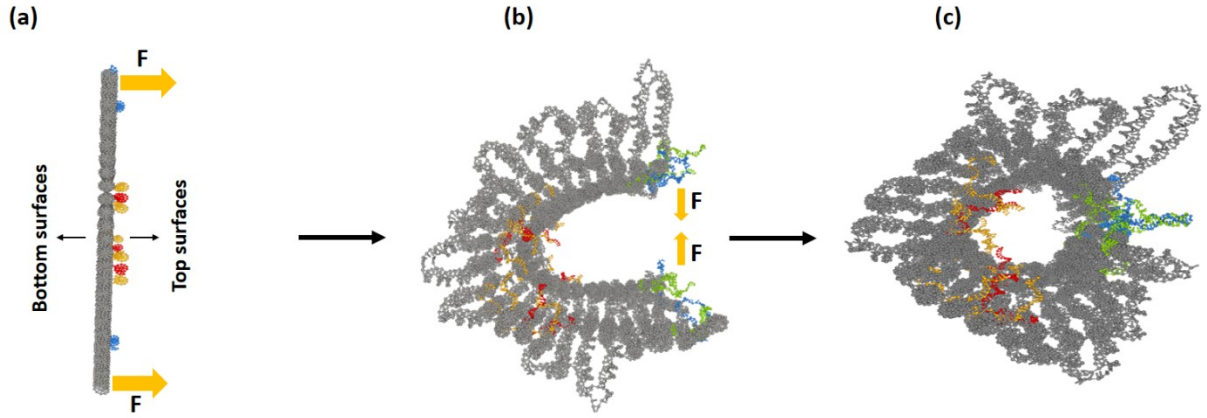

Figure S2. Two-step closure of the DNA origami nanosheet visualized in oxView.

(a) A harmonic pulling bias was applied perpendicular to the nanosheet plane to bring opposing scaffold termini into contact. (b) Once the edges approached, complementary aptamer base pairing was emulated using mutual harmonic traps between paired locking strands. (c) Final locked nanosheet configuration.

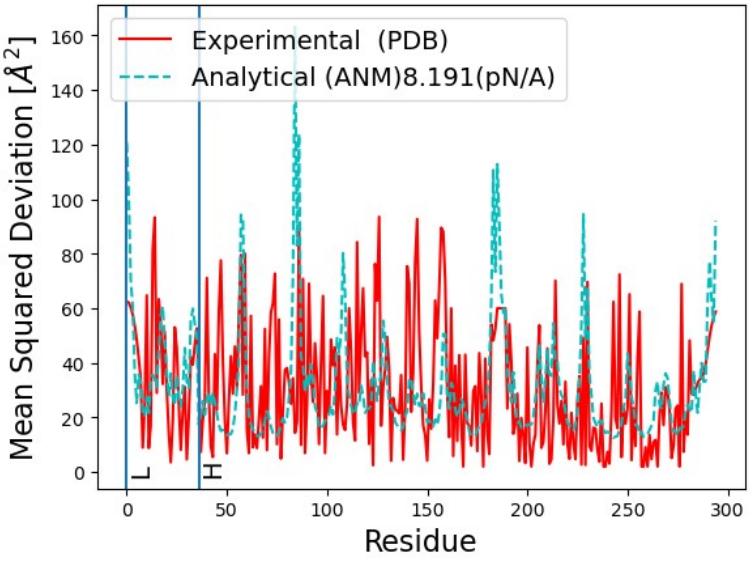

Figure S3. B-factor profile and ANM validation for thrombin.

Residue-level thermal fluctuation profile of the ANM thrombin model compared with experimental B-factors obtained from the corresponding PDB structure. The plot was generated directly using the ANM–oxDNA package to validate the coarse-grained protein representation.

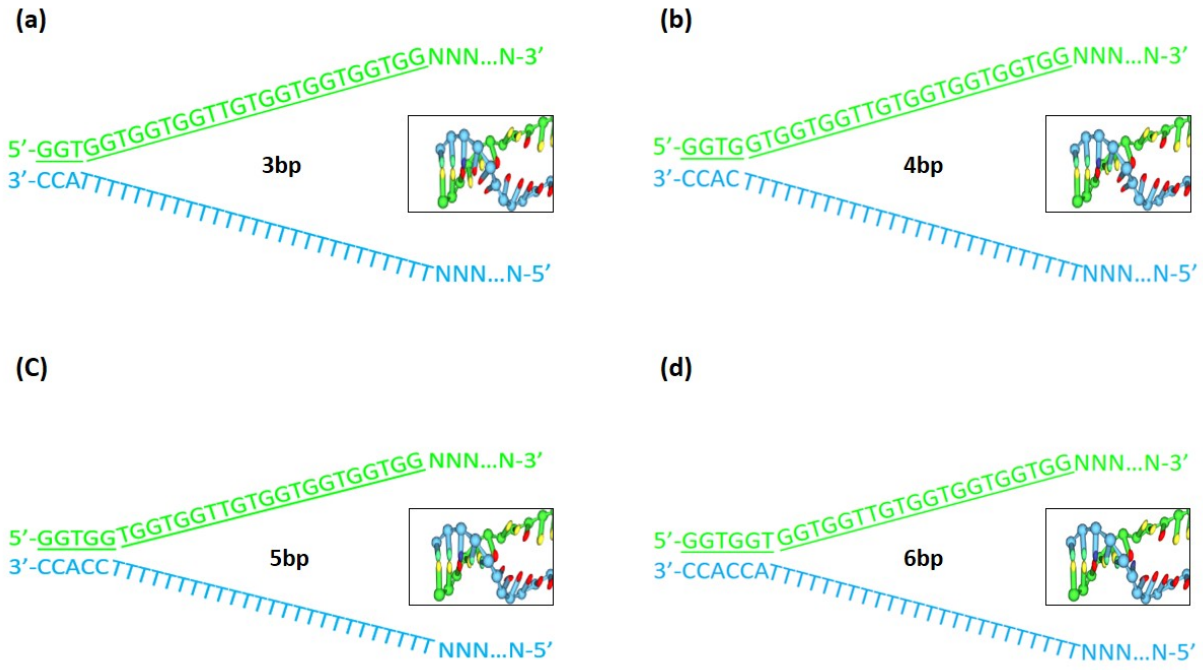

Figure S4. Sequence designs of locking strands with different duplex lengths.

(a–d) Complementary lock–aptamer domains designed for 3-, 4-, 5-, and 6-bp duplexes, respectively. These variants were employed to investigate the effect of duplex length on lock stability and unlocking kinetics.

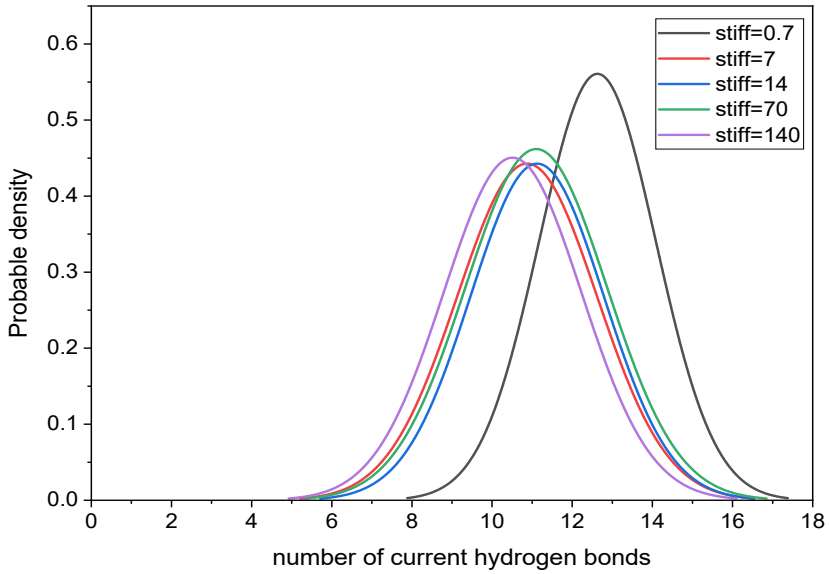

Figure S5. Sensitivity of linker hydrogen-bond stability to harmonic trap stiffness. Probability distributions of the number of correctly formed hydrogen bonds for a representative thrombin–linker complex obtained from

equilibrium oxDNA simulations using different harmonic trap stiffness values (0.7–140, oxDNA units). The complementary DNA strand was held fixed to isolate the effect of restraint strength. Very low stiffness (0.7) results in enhanced fluctuations, whereas stiffness values ≥7 yield convergent hydrogen-bond distributions, indicating robustness of linker stability to moderate variations in trap stiffness.